Pulse-Triggered Instability in Solid Rocket Motors

Joseph D. Baum* and Jay N. Levine†
Air Force Rocket Propulsion Laboratory/DYC, Edwards Air Force Base, California
and
Richard L. Lovine‡
Aerojet Tactical Systems, Sacramento, California

This paper presents the results of a study to assess the ability of a recently developed comprehensive nonlinear combustion instability model to predict pulse-triggered instability in solid rocket motors. Performance models were developed to calculate the mass and energy flow rates produced by three laboratory pulsers (pyro, low brisance, and piston). The mass and energy flow rates are utilized as boundary conditions for the comprehensive nonlinear combustion instability model. The model predicts the temporal and spatial evolution of the resulting waveforms (amplitude and harmonic content) in the combustion chamber. Comparisons of theoretical predictions with experimental data for both laboratory and full-scale motors are presented. Very good agreement is demonstrated between the predicted and measured pulse amplitudes, wave shapes, limiting amplitudes, mean pressure shifts, and growth rates.

Introduction

SOLID propellant rocket motors can experience several types of combustion instability; e.g., high or low frequency, longitudinal or tangential, linear or nonlinear. Nonlinear instability is one of the more troublesome, especially for current reduced or minimum smoke tactical solid propellant rocket motors. Such instabilities are usually characterized by large amplitude oscillations having steep-fronted, shock-like waveforms, and are often accompanied by significant increases in mean chamber pressure.

In flight, nonlinear combustion instability can be triggered by random finite amplitude events such as the expulsion of an igniter or insulation fragment through the nozzle. In the laboratory, this phenomenon is simulated using laboratory pulsers. The concept of evaluating motor stability by pulsing has been utilized in the past to test both liquid and solid propellant rocket motors.[1-4] However, the physical mechanisms responsible for the pulse initiation of nonlinear instability are not yet fully understood. As a result of the complexity of this phenomenon, efforts to analytically model and predict pulse-triggered instability have been limited compared to the extensive analytical work that has been devoted to linear instability problems.

Prior to the present work, existing nonlinear combustion instability analyses[5-8] were not capable of treating the multiple traveling shock wave type of instabilities that occur in reduced smoke variable cross-sectional area solid rocket motors. In addition, the existing analyses were not capable of treating velocity coupling effects. During the course of the present investigation, the most advanced model[5] was modified and extended to overcome the deficiencies which preclude it from predicting pulse-triggered instability. The resulting comprehensive model of nonlinear longitudinal combustion instability is described in Ref. 9. The two primary elements of this stability analysis are a finite difference solution of the two-phase flow in the combustion chamber and a coupled solution of the nonlinear transient propellant burning rate. Although quasi-one-dimensional, the model has been generalized to treat realistic variable cross-section and partial length grains.

The most significant improvements incorporated into the present analysis were an advanced finite difference integration scheme and an ad hoc velocity coupling model. The tendency of "older" shock-capturing finite difference integration techniques[10,11] to produce spurious pre- and post-shock oscillations which could falsely trigger combustion instabilities was overcome by utilizing a recently developed scheme based on a combination of the Lax-Wendroff,[12] Hybrid,[13] and Artificial Compression[14] schemes. The ability of the LW + H + ACM finite difference scheme to yield sharp and oscillation-free transitions of both shocks and contact discontinuities and to accurately calculate propagation of multiple shock waves in variable area combustion chambers has been demonstrated.[15,16]

From a review of existing models of velocity coupling,[17,18] it was concluded that all existing models have significant deficiencies and are not based on an understanding of the fundamental physical mechanisms. However, in order to explore the role of velocity coupling in triggered instability, and to demonstrate the ability of the present comprehensive stability analysis to serve as a basis for assessing the validity of future improved transient combustion models, ad hoc velocity coupling models were incorporated into the analysis.[18] The ability of the overall model to qualitatively predict all of the nonlinear phenomena observed in actual solid rocket motor firings—e.g., triggering of a nonlinear instability by a finite amplitude pulse, shifts in the mean motor operating pressure, modulated amplitude limit cycles, and strongly nonlinear traveling waves (shocks)—has been demonstrated.

Ballistic models of the pyro, low brisance, and piston pulsers were developed utilizing a simple lumped volume treatment.[19] The mass and energy flow rates calculated using these pulser performance models are utilized as boundary conditions for the combustion chamber flow problem. The comprehensive nonlinear combustion instability program[9] that solves the partial differential equations that govern the associated flow and combustion instability in solid propellant rocket motors was then modified to model the effect of fore-end pulsing based on the mass and energy flux data provided by the pulser ballistic analysis. The ability of the combined

Presented as Paper 82-1219 at the AIAA/SAE/ASME 18th Joint Propulsion Conference, Cleveland, Ohio, June 21-23, 1982; submitted Nov. 1, 1982; revision received Oct. 31, 1983.

*Research Scientist. Member AIAA.
†Research Physical Scientist.
‡Engineering Specialist. Member AIAA.

pulser/chamber model to accurately predict the pulse-induced waveforms (amplitude and harmonic content) in closed chambers filled with cold gases has been demonstrated.[20]

The excellent results demonstrated in these studies led to the investigation reported herein, which is an evaluation of the ability of the overall pulser and nonlinear stability model to predict pulse-triggered instability in both laboratory and full-scale rocket motors. The ability of the present analysis to predict a priori the nonlinear stability of motors is inhibited by deficiencies in existing pressure and velocity coupling combustion response models. Modeling deficiencies are further exacerbated by the lack of accurate measured values for key propellant parameters such as surface temperature, activation energy and net heat release rate of the surface decomposition reaction, thermal diffusivity, etc. Moreover, as pointed out previously, existing velocity coupling models, including the present ad hoc model, are not based on an understanding of the fundamental physical mechanisms. Given the present state of combustion response modeling, the key issues to be addressed in this investigation were: the ability of the overall model to predict the relative nonlinear stability of motor/propellant combinations as a function of grain geometry, operating conditions, and pulse amplitudes (for a fixed propellant formulation); and the ability of the model to predict all of the nonlinear characteristics observed in motor firing data. The first issue was addressed by comparing predictions and measured data for a series of laboratory scale motor firings. The second issue was addressed by comparing predictions and data for both laboratory and full-scale motor firings. Comparisons of theoretical predictions with experimental data from a series of laboratory scale tests and for two full-scale motors are presented.

Laboratory Scale Motors

A series of experiments was carried out in which several laboratory scale motors with the same propellant and different grain geometries and nozzles were pulsed by different pulsers at different operating pressures.

The test motors were 1.22 m (48 in.) long and had an internal case diameter of 5.71 cm (2.25 in.). Partial length grains were located at the fore-end of the motor. The grains were partially recessed into the case. Thus, at some time toward the end of a firing, a flush grain configuration was achieved. Prior to this time the grain represents an area constriction, and after this time the grain is recessed relative to the case diameter. Two types of pulsers were used in the tests to be reported herein, i.e., pyrotechnic and piston pulsers.[19] Two pulser units were attached to the fore-end of the motor for each test.

Instrumentation

The pressure oscillations in the motor were recorded at six axial locations using Kistler Model 703 piezoelectric pressure transducers. A single dc transducer was used to record mean pressure. The transient pressures in the breech of the pulse units were also measured with piezoelectric transducers. Thermal shielding of the pressure transducers was accomplished using vulcanized rubber (RTV). Based on shock tube calibration tests, it was concluded that an RTV thickness of 0.317 cm (0.125 in.) yields optimal resolution of the high-frequency content of steep-fronted shock waves within the constraint of adequate insulation. With a 0.317 cm (0.125 in.) RTV coating, the resonant frequency of the transducer is reduced from approximately 90 kHz to about 64 kHz with an amplitude accuracy within ~10%. At this level, high-frequency measurements can be obtained up to about 20 kHz. Nevertheless, artificial oscillations at very high frequencies that are observed in the transducer response immediately following the passage of a shock wave could not be completely eliminated. Therefore, the measured pulse amplitudes reported herein were corrected for this effect, in an approximate manner, whenever present.

Pulse Predictions

The ability of the combined pulser/chamber model to accurately predict the pulse-induced waveforms in closed chambers filled with cold inert gases has been demonstrated. The validity of the pulser modeling under actual motor firing conditions was examined in this study.

Test PCC3 utilized a grain length of 22.8 cm (9 in.) and an initial internal grain diameter of 3.17 cm (1.25 in). Two piston pulsers, each having 0.7 g of Red Dot powder but different stroke lengths, were used. The pulse units were fired at motor burn times of 0.95 and 1.17 s, when the mean pressure was 10.37 and 11.45 MPa (1503 and 1660 psi), respectively. Figures 1a and 1b compare the measured and predicted pulser breech pressure time histories for the two pulses. Very good agreement was obtained for the primary pulse; however, the analysis cannot predict the small secondary pressure variation

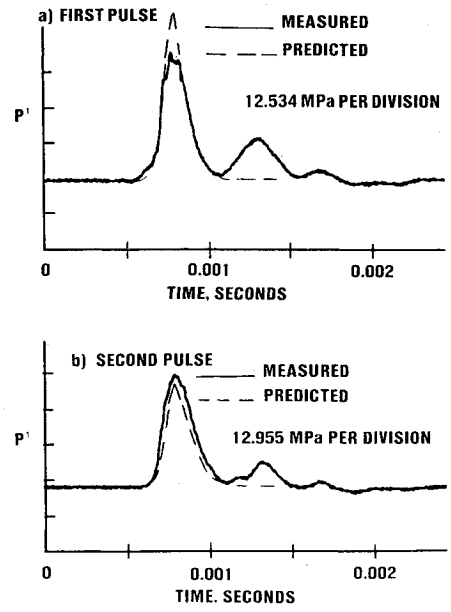

Fig. 1 Comparison of measured and predicted piston pulser breech pressures, test PCC3.

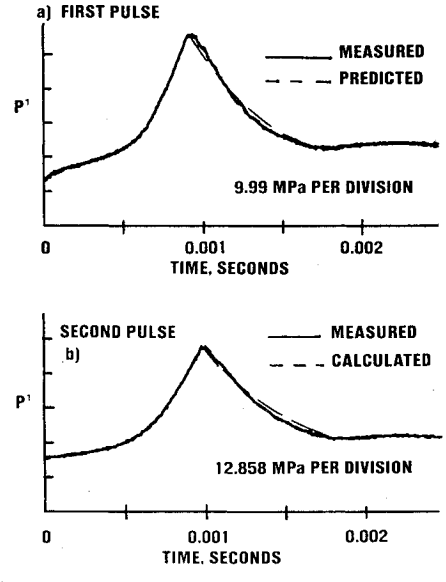

Fig. 2 Comparison of measured and predicted pyro pulser breech pressures, test PCC4.

that is produced in some cases when the piston bounces off the lead stop instead of sticking to it.

Test PCC4 utilized a grain length of 20.32 cm (8 in.) and an internal grain diameter of 3.17 cm (1.25 in.). In this test two pyro pulsers, having 0.165 g of Red Dot powder, were fired 0.98 and 1.21 s into the motor firing, at chamber pressures of 11.12 and 12.25 MPa (1612 and 1776 psi), respectively. Figures 2a and 2b show a comparison of the measured and predicted breech pressure time histories. Excellent agreement was obtained, demonstrating the ability of the pulser performance model to predict the breech pressure, and, consequently, the mass and energy flux rates into the combustion chamber.

It will be shown in the next subsection that, when the mass and energy flux rates calculated using the piston and pyro pulser performance models were used as boundary conditions for the nonlinear stability analysis, excellent agreement between the predicted and measured pulse amplitudes and waveforms was also obtained. These results, as well as the results of additional comparisons not reported herein, demonstrate the ability of the pulser/chamber model to accurately predict the pressure perturbations produced by laboratory pulse units.

Stability Predictions

It was noted previously that several of the parameters that determine the pressure-coupled vs frequency characteristics of the burning propellant are unknown. To overcome this deficiency, this set of parameters and the magnitude of the velocity-coupled response were chosen to yield a best fit for pulse 1 of test PCC3. This test was established as the baseline, and all of the other stability predictions were carried out leaving these values unchanged. All of the parameter values utilized were physically reasonable.

The time evolution of the chamber pressure for test PCC3, measured by a Taber transducer located at the fore-end, is shown in Fig. 3. The motor was stable in response to the first pulse and was driven unstable in response to the second pulse. The measured fore-end pressure oscillations induced in the motor by the first pulse are shown in Fig. 4a. The first piston pulser-induced wave has an amplitude of 0.724 MPa [(105 psi) or 7% of the mean pressure]. It should be noted that all initial pulse amplitudes are quoted based on the first reflection of the wave from the aft end. The initial shocked waveform rapidly decays to an almost sinusoidal waveform, indicating that the motor is stable to this pulse (i.e., the motor could not sustain a nonlinear instability). The predicted time evolution of pressure oscillations for this case, obtained by utilizing the predicted mass and energy flow rates as boundary conditions for the nonlinear combustion instability program, is shown in Fig. 4b. The set of parameters listed in column a of Table 1 was utilized in this baseline test. A and B are transient burn rate parameters defined in Ref. 5 and P is the mean chamber pressure. Excellent agreement is demonstrated between the measured and predicted initial pulse amplitude and waveform, the decay rate of the pulse, and the temporal evolution of the waveform's decay rate and harmonic content of the waves. The temporal evolution of the waveform, as observed in both the predicted and the measured data, is of special interest. The generation of a second shock wave is attributed to partial reflection from the area discontinuity at the end of the solid propellant grain, a discontinuity that still exists at the time the first pulse is fired. This reflected shock wave is initially amplified in time as the original pulse decays, until it dominates the waveform.

Since the gases injected from the piston pulser are at a significantly lower temperature than the gases in the hot motor, a large temperature gradient is formed near the fore-end, resulting in the formation of an expansion wave behind the propagating shock. This phenomenon is observed in both the measured and predicted data. In the experiment, the mixing of the hot propellant products with the cold gases reduces the temperature gradient rapidly. The current analysis does not treat mixing, thus the calculated temperature gradient remains unrealistically steep for a relatively longer

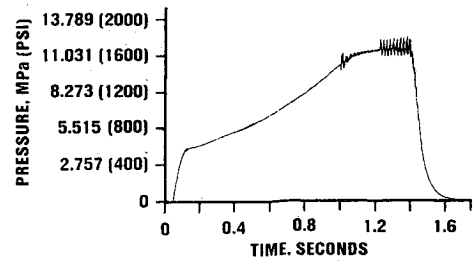

Fig. 3 Chamber pressure as a function of time, test PCC3.

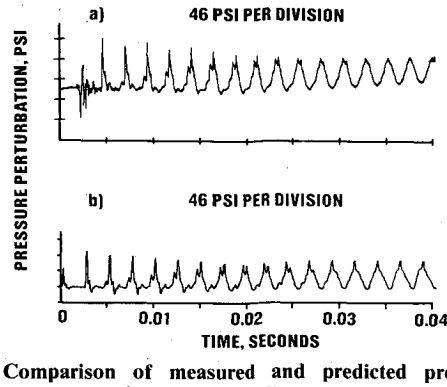

Fig. 4 Comparison of measured and predicted pressure perturbations at the fore-end, test PCC3, first pulse.

Table 1 Propellant parameters values

Burn rate, in./s	$0.3899\left(\frac{\bar{P}}{1000}\right)^{0.43}$	$0.35\left(\frac{\bar{P}}{1000}\right)^{0.45}$	$0.30\left(\frac{\bar{P}}{1000}\right)^{0.43}$	$0.31\left(\frac{\bar{P}}{1000}\right)^{0.40}$
Density of solid propellant, g/cm^3	1.71895	1.71895	1.81895	1.713415
Thermal diffusivity of propellant, cm^2/s	0.00266461	0.00257327	0.0016129	0.0016129
Adiabatic flame temperature, °R	5378.0	5378.0	5364.0	5274.0
Gas only specific heat, Btu/lb°R	0.4568	0.4568	0.4568	0.4565
Gas only isentropic exponent	1.2	1.2	1.2	1.208
Propellant steady-state surface temperature, °R	1454.2	1454.2	1454.2	1454.2
Propellant back wall temperature, °R	543	543.0	624.67	543
Propellant only specific heat, Btu/lb°R	0.305	0.305	0.305	0.305
A	5.0	11.5	20	6.0
B	0.53	0.86	1.06	0.66
Linear pressure-coupled response, R_{pc}	1.092	1.53	1.32	1.344
Velocity-coupled response, R_{vc}	3.0	3.0	6.0	5.6

period of time (about seven wave cycles in the predicted data as compared to about four in the measured data). In contrast, when hot gases are injected into a cold chamber,[20] an expansion is developed in front of, rather than behind, the shock.

The measured fore-end pressure oscillations for test PCC3 pulse 2 are shown in Fig. 5a. In this case, the piston pulser produced a pulse having an amplitude of about 0.43 MPa [(63 psi) or 3.8% of the mean pressure]. The predicted pressure history is shown in Fig. 5b. The predicted pulse amplitude (3.8%) and waveform, as well as the temporal evolution of the waves (shape, amplitude, and growth rate) are all in excellent agreement with the measured data. For instance, after 15 wave cycles, both the measured and predicted waves have an amplitude of 5.2% of the mean pressure. Without changing any of the parameters (Table 1, column a) from those employed in predicting the first pulse, the analysis was able to correctly predict that the second pulse would trigger a sustained nonlinear instability.

In the second motor firing considered (PCC4), pyro pulsers were employed instead of piston pulsers, the grain was shortened to 20.32 cm (8 in.), and the nozzle diameter was reduced. The mean pressure history for this test is shown in Fig. 6. The pulsers were fired at 0.98 and 1.21 s into the motor firing at mean pressures of 11.12 and 12.25 MPa (1612 and 1776 psi), respectively. At these conditions, the motor is marginally unstable—in a linear sense—at the second mode frequency, and low level spontaneously initiated oscillations are observed throughout the firing. As in test PCC3, the first pulse of test PCC4 failed to produce sustained nonlinear oscillations, while the second pulse did trigger a nonlinear instability.

Figures 7a and 8a show the measured time evolution of pressure oscillations at the fore-end of the motor induced by the two pulses. The corresponding calculated results are shown in Figs. 7b and 8b. Despite the presence of the residual spontaneous second-mode oscillations, which are unaccounted for in the analytical results, the predicted and measured initial pulse amplitudes and waveforms, and the wave growth rate (second pulse) and decay rate (first pulse) are all in very good agreement. The amplitude of the first pulse was measured to be 2.5% of the mean pressure, while the predicted value was 2.6%. For the second pulse the measured value was 2.3% and the predicted amplitude was 2.4%. Here again, the analysis was successful in predicting the motor response to each of the pulses. After the first pulse, both the data and predictions show that the pressure oscillations first increase for about six wave cycles and then decay slowly. The amplitude of the second pulse was near the limit cycle amplitude; hence, the pressure oscillations increase only slightly following the pulse. In both cases, the measured and predicted wave amplitudes at the end of 15 wave cycles are in very good agreement.

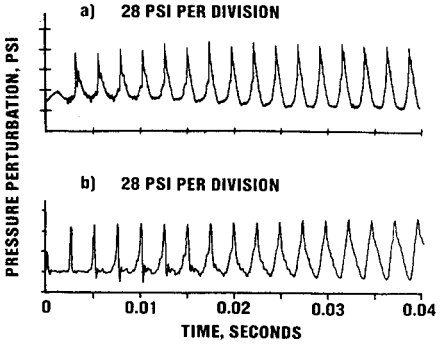

Fig. 5 Comparison of measured and predicted pressure perturbations at the fore-end, test PCC3, second pulse.

The third and last set of data obtained in this series of tests, test PCC2, was also conducted with a 20.32 cm (8 in.) long grain, but at significantly lower chamber pressures. Two piston pulse units were fired during this test at chamber pressures of 8.84 and 10.21 MPa (1282 and 1481 psi). The first pulse, with an initial amplitude of about 0.33 MPa [(48 psi) or 3.74% of the mean pressure], decayed rapidly into a sinusoidal waveform. The results were qualitatively similar to those obtained in test PCC3, but with a somewhat larger decay rate. The second pulse, with an amplitude of 0.4 MPa [(58 psi) or 3.9% of the mean pressure], initially increased in amplitude (to about 4.6% of the mean pressure after six wave cycles), but then decayed. Thus, at the lower pressures used in PCC2, both pulses were stable. The theoretical predictions for this motor indicated very good agreement with the measured data. The prediction indicated that the motor will be stable in response to both pulses and the analysis correctly predicted that the first pulse would decay rapidly and that the second pulse would grow initially and then decay slowly. The initial pulse amplitudes and waveforms were also accurately predicted. The measured data for PCC2 pulse 1 demonstrated reflected wave behavior (from the area discontinuity at the end of the grain) similar to that observed in response to the first pulse of test PCC3. This observed behavior was again correctly predicted by the analysis.

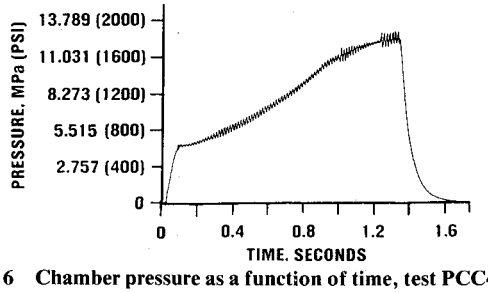

Fig. 6 Chamber pressure as a function of time, test PCC4.

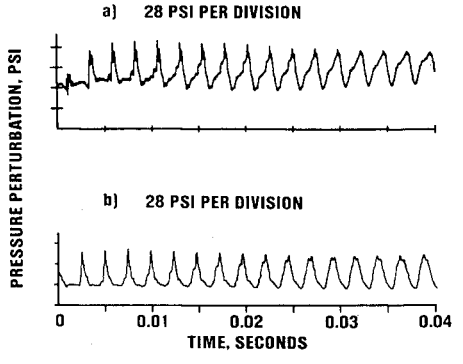

Fig. 7 Comparison of measured and predicted pressure perturbations at the fore-end, test PCC4, first pulse.

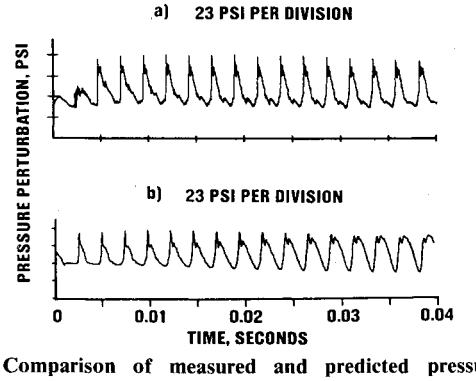

Fig. 8 Comparison of measured and predicted pressure perturbations at the fore-end, test PCC4, second pulse.

observed in response to the first pulse of test PCC3. This observed behavior was again correctly predicted by the analysis.

Before applying the nonlinear analysis to the prediction of nonlinear instability in full-scale motors, an additional laboratory scale motor comparison was conducted with a more complex and motor-like grain distribution than those employed in the previous tests. The propellant distribution along the chamber for test firing 4 is depicted in Fig. 9. A pyro pulser (attached to the fore-end) generated a pulse, at the time when the propellant burned back to a flush condition, with an amplitude of 5.1% of the 9.897 MPa (1435 psi) mean pressure. The time evolution of the measured and predicted pressure oscillations at the fore-end are shown in Fig. 10. Excellent agreement is demonstrated between the measured and predicted data. The initial pulse amplitude was predicted to be 5.1% of the mean pressure, in agreement with the measured value. After 15 wave cycles, the amplitude of both measured and predicted waves was 6.2% of the mean pressure. In addition, the measured and predicted waveforms are very similar. It should be mentioned that the composition of the propellant in test 4 was slightly different than that utilized previously. The propellant parameters utilized to predict the pressure-time data for this case are shown in Table 1, column b.

In the laboratory scale tests discussed above, only small ($\pm 1\%$) instability-induced mean pressure shifts were observed. The analytical solutions for these cases also predicted only small shifts in mean pressure.

Full-Scale Motors

An assessment of the validity of the present nonlinear instability model would not be complete without examining its ability to predict nonlinear instability in full-scale motors. Data from two motor firings were selected for use in the present comparison study. Motors A and B, as they will be termed, were development reduced smoke motor designs. Both motors were stable until pulsed, were pulse triggered into sustained nonlinear instability, and exhibited shifts in mean pressure after pulsing.

Details of the pulser designs utilized to pulse these motors were not available. Thus, predictions were obtained by varying the input mass flux until the experimentally observed pulse amplitude was reproduced. As in the case of the baseline laboratory scale motor, the parameters that control the characteristics of the pressure and velocity combustion response as a function of frequency were varied to obtain the best agreement possible. It should be recalled that the issue to be addressed in this study was the capability of the present analysis to predict all of the nonlinear characteristics observed in full-scale motor instability data and not the capability to a priori predict motor response to pulses.

Motor A

A number of different grain designs and propellants were tested during this motor development program. The motor selected for this comparison study had a five-point gear grain configuration, and a grain length of 1.65 m (65 in.). The propellant utilized was an AP oxidized reduced smoke propellant containing a small amount of stability additive. The motor was pulsed with a piston pulser 2.5 s into the firing when the chamber pressure was 10.69 MPa (1550 psi). The cross-sectional area and cumulative burn surface area at the time of pulsing are plotted in Fig. 11. For the sake of computational efficiency, certain small details of the grain distribution were modified. A single fore-end mounted transducer (Kistler Model 603A) was used to monitor the pressure oscillations. The transducer had a 0.25 cm (0.1 in.) coating of RTV for thermal protection and a stand-off distance of 2.29 cm (0.9 in.). In its mounted configuration, the transducer had a resonant frequency of about 6000 Hz.

The measured time evolution of the pressure oscillations following the pulse is shown in Fig. 12a. Although not evident in this figure (dc pressure changes were filtered out), the motor experienced a 10.9% increase in mean pressure (dc shift) as a result of the pulse-induced instability. The waveform of the pressure oscillations is quite nonlinear, and is primarily a single traveling shock wave. The combination of a shocked waveform, with its attendant large high-frequency content, and the low resonant frequency of the Kistler transducer in its mounted configuration, resulted in transducer resonance (or ringing) and distortion of the true waveform. This phenomenon is more clearly evident when the analog tape is speed-scaled before digitization and plotting. The presence of this ringing precludes the accurate quantization of the wave amplitude, but hand correction for this effect (see Fig. 12b) produces a wave history that is satisfactory for the present qualitative comparison study.

The parameters shown in Table 1, column c, were utilized as input data for the nonlinear combustion instability model. The predicted time evolution of the pressure oscillations is shown in Fig. 12c. Excellent agreement between the measured and predicted data was obtained. Both the predicted and measured oscillations grew from the initial pulse amplitude of 3.4% to amplitudes between 22 and 24% after 11-13 wave cycles, and decreased slightly afterwards. The predicted dc

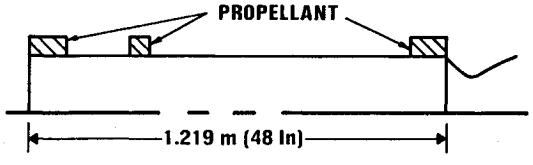

Fig. 9 Propellant grain distribution, test 4.

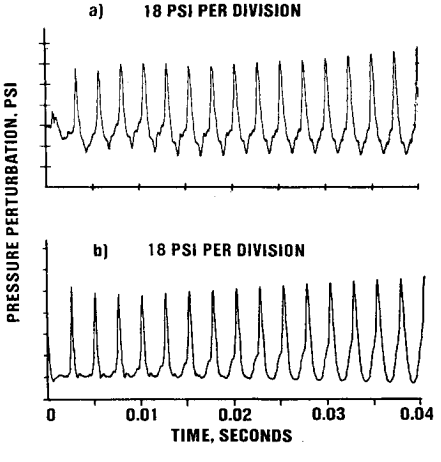

Fig. 10 Comparison of measured and predicted time evolution of pressure perturbations at the fore-end, test 4, second pulse.

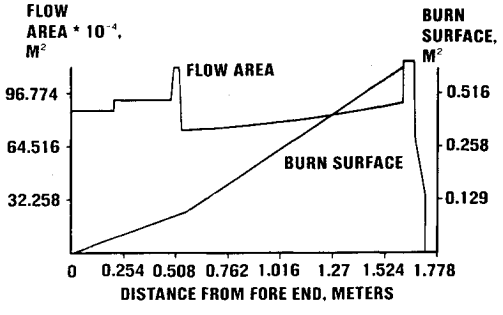

Fig. 11 Motor A; axial variation of flow area and cumulative burn surface area.

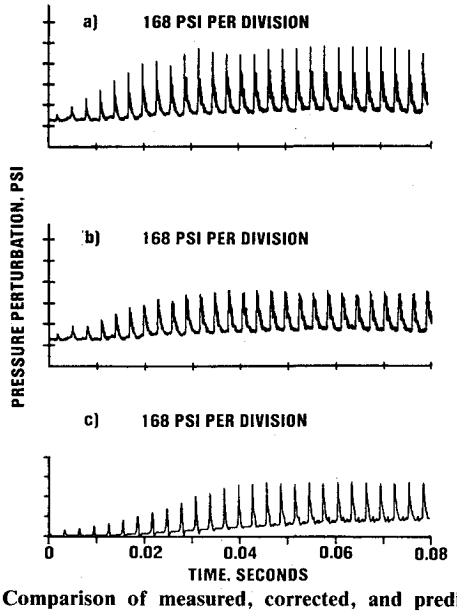

Fig. 12 Comparison of measured, corrected, and predicted time evolution of pressure oscillations at the fore-end, motor A.

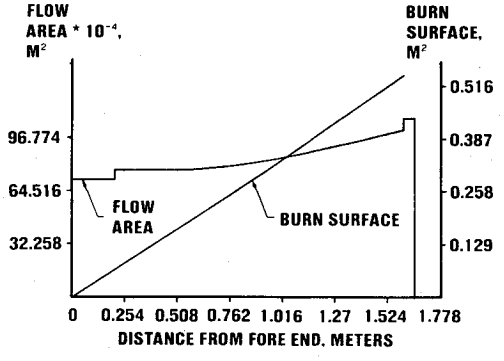

Fig. 13 Motor B; axial variation of flow area and cumulative burn surface area.

pressure shift (11%) and the predicted wave shape were also both in close agreement with the experimental data.

Motor B

During development work on motor B, a number of motors were pulse tested to determine their nonlinear stability. The motor selected for this study had a fore-end finocyl grain configuration with three fins. The motor had a grain length of 166.4 cm (65.5 in.) and a fin length of 55.88 cm (22 in.). An AP oxidized reduced smoke propellant containing a burn rate retardant was utilized in this test. The motor was pulsed with a pyro pulser 2.78 s into the firing when the chamber pressure was 5.38 MPa (780 psi). The cross-sectional area and cumulative burn surface area, at the time of pulsing, are plotted in Fig. 13. Each motor was instrumented with two Taber transducers for mean pressure measurement, three accelerometers, and a Kistler 606A high-frequency transducer located at the fore-end closure. The Kistler was recessed about 1.78 cm (0.7 in.) and was protected by a 0.25 cm (0.1 in.) coating of RTV. The resonant frequency of the transducer was in the range of 5-10 kHz.

It can be seen from the fore-end pressure oscillation history, presented in Fig. 14a, that the instability data for this motor are also compromised by transducer ringing. These results demonstrate the importance of keeping the transducer

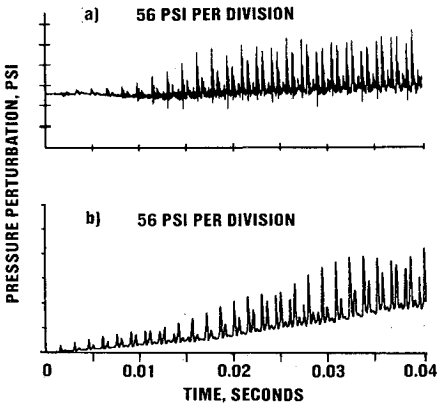

Fig. 14 Comparison of measured and predicted time evolution of pressure perturbations at the fore-end, motor B.

resonance frequency as high as possible in future pulse testing of solid motors.

The time evolution of the pressure oscillations for motor B is more complex than that of motor A, and is characterized by the presence of multiple, variable amplitude shock waves. Thus, correcting the data for transducer ringing becomes fairly subjective. Nevertheless, it is possible to approximate the true response by mentally removing the thin spike-like top portion of each wave front. As in the laboratory scale motor firings, the complexity and multiple shock wave nature of motor B's pressure history is attributed to partial wave reflections from an internal area discontinuity in the chamber. In motor B (Fig. 13) the only sizable flow area discontinuity is located approximately one-third of the way between the fore-end and the end of the grain. Correspondingly, the multiple shock waves are spaced at intervals approximately equal to one-third of a full wave cycle. It should be mentioned, however, that while not presented herein, existing data and analytical results show that multiple shock waves can also be driven by propellant combustion, e.g., when the propellant transient response is much higher at second or higher longitudinal mode frequencies than at the fundamental mode.

The propellant parameters shown in Table 1, column d, were utilized in obtaining the analytically predicted pressure oscillation history for motor B shown in Fig. 14b. Comparing Figs. 14a and 14b, it is noted that the theoretical results qualitatively reproduce the complex tertiary shock wave behavior present in the experimental data. Both the experimental and predicted wave histories contain two relatively stronger shock waves and one weak shock wave. In the predicted data a repetitive pattern is observed in which the weaker of the two dominant waves grows until it becomes the larger shock wave. In the experimental data, the relative amplitudes of the two larger shock waves vary in time, but not in as cyclical a manner. Relatively good agreement between the predicted and measured wave amplitudes and mean pressure shifts was obtained. Both the measured and predicted dc shifts were approximately 10% of the chamber pressure (the dc shift in the experimental data was filtered out and is not discernible in Fig. 14a).

Conclusions

On the basis of the comparisons with motor firing data carried out to date, the following conclusions have been drawn:

1) The comprehensive nonlinear combustion instability model developed during the present investigation appears to be capable of predicting all of the nonlinear phenomena observed in both laboratory and full-scale motors, including multiple shock wave instabilities in motors containing complex grain configurations.

2) The ability of the developed pulser/chamber model to accurately predict a priori both initial pulse amplitude and waveform, under actual solid rocket motor firing conditions, has been demonstrated.

3) When the parameters which control the pressure and velocity coupled propellant response were empirically fixed on the basis of a single "baseline" pulse test, the nonlinear model was shown to be able to quantitatively predict the measured nonlinear stability of five other pulse tests with the same propellant, but with varying grain geometry, operating conditions, pulser types, and pulse amplitudes. Thus, the present analysis should provide a useful preliminary design tool for predicting the relative nonlinear stability of candidate motor design variations. With further advances in combustion response modeling, the nonlinear model should eventually provide an a priori means for quantitatively predicting the nonlinear longitudinal stability of solid rocket motors.

4) In view of the known deficiencies in the combustion response models utilized, the ability of the analysis to simultaneously match measured wave amplitudes, waveforms, dc shifts, and, in many cases, growth (or decay) rates, were satisfying, although somewhat surprising. It seems likely, therefore, that the present combustion models at least contain all of the essential factors which produce the nonlinear behavior that can be attributed to the propellant response.

5) Many of the complexities observed in unstable motor oscillations are caused, or strongly influenced, by discontinuities in the grain geometry. This is especially true for multiple shock wave behavior induced by partial shock wave reflection at area discontinuities.

6) It is strongly recommended that great care be taken in future motor pulse testing to ensure that the piezoelectric pressure transducers are mounted and protected in a manner that will keep the resonant frequency of the transducer as high as possible. Resonant frequencies above 60 kHz should be sought in order to keep transducer "ringing" effects from significantly compromising the integrity of the data.

7) Additional comparisons with motor data should be carried out to further evaluate the ability of the present analysis to predict the effect of grain design, pulse type, and pulse amplitude, for a wider range of propellants, motor operating conditions, and pulse characteristics than contained herein.

Acknowledgment

This work was partially supported under Air Force Contract F04611-81-C-0012.

References

[1] Combs, L.P. et al., "Improvement of Bombs and Pulse Guns as Combustion Stability Ratings Devices," AFRPL-TR-68-018, March 1968.

[2] Dickinson, L.A., "Command Initiation of Finite Wave Axial Combustion Instability in Solid Propellant Rocket Motors," *ARS Journal,* Vol. 32, 1962, p. 643.

[3] Hughes, P.M. and Smith, D.L., "Nonlinear Combustion Instability in Solid Propellant Rocket Motors; Influence of Geometry and Propellant Formulation," 53rd AGARD Meeting, Propulsion and Energetics Panel, Oslo, Norway, April 1979.

[4] Morris, E.P., "A Pulse Technique for the Evaluation of Combustion Instability in Solid Propellant Rocket Motors," *CAS Journal,* 1965, pp. 329-333.

[5] Levine, J.N. and Culick, F.E.C., "Nonlinear Analysis of Solid Rocket Combustion Instability," AFRPL TR-74-45, Oct. 1974.

[6] Kooker, D.E. and Zinn, B.T., "Numerical Investigation of Nonlinear Axial Instabilities in Solid Rocket Motors," Ballistic-Research Laboratories, CR 141, March 1974.

[7] Culick, F.E.C., "Nonlinear Behavior of Acoustic Waves in Combustion Chambers," CPIA Pub. 243, 10th JANNAF Combustion Meeting, Vol. 1, 1973, pp. 417-436.

[8] Powell, E.A., Padmanabahn, M.S., and Zinn, B.T., "Approximate Nonlinear Analysis of Solid Rocket Motors and T-Burners," AFRPL-TR-77-48, 1977.

[9] Levine, J.N. and Baum, J.D., "Modelling of Nonlinear Combustion Instability in Solid Propellant Rocket Motors," *Proceedings of the Nineteenth International Symposium on Combustion,* Haifa, Israel, Aug. 1982, pp. 769-776.

[10] Rubin, E.L. and Burstein, S.Z., "Difference Methods for the Inviscid and Viscous Equations of a Compressible Gas," *Journal of Computational Physics,* Vol. 2, 1967, pp. 178-196.

[11] MacCormack, R.W., "Proceedings of the Second International Conference on Numerical Methods in Fluid Dynamics," *Lecture Notes in Physics,* edited by M. Holt, Vol. 8, Springer-Verglag, New York, 1971.

[12] Lax, P.D. and Wendroff, B., "System of Conservation Laws," *Communications on Pure and Applied Mathematics,* Vol. 13, 1960, pp. 217-237.

[13] Harten, A. and Zwas, G., "Self Adjusting Hybrid Schemes for Shock Computations," *Journal of Computational Physics,* Vol. 9, 1972, pp. 568-583.

[14] Harten, A., "The Artificial Compression Method for Computation of Shocks and Contact Discontinuities: III, Self Adjusting Hybrid Schemes," AFOSR TR-77-0659, March 1977.

[15] Baum, J.D. and Levine, J.N., "Evaluation of Finite Difference Schemes for Solving Nonlinear Wave Propagation Problems in Rocket Combustion Chambers," AIAA Paper 81-0420, Jan. 1981.

[16] Levine, J.N. and Baum, J.D., "A Numerical Study of Nonlinear Instability Phenomena in Solid Rocket Motors," AIAA Paper 81-1524, July 1981.

[17] Beckstead, M.W., "Report of the Workshop on Velocity Coupling," CPIA Report 324, 17th JANNAF Combustion Meeting, NASA Langley Research Center, Hampton, Va., Nov. 1980.

[18] Levine, J.N. and Baum, J.D., "A Numerical Study of Nonlinear Instability Phenomena in Solid Rocket Motors," *AIAA Journal,* Vol. 21, April 1983, pp. 557-564.

[19] Lovine, R.L., "Nonlinear Stability for Tactical Motors – Pulsing Considerations," CPIA Report 347, 18th JANNAF Combustion Meeting, Pasadena, Calif., Oct. 1981.

[20] Baum, J.D., Lovine, R.L., and Levine, J.N., "Pulsing of Solid Propellant Rocket Motors: A Numerical and Experimental Study," AIAA Paper 82-0359, Jan. 1982.